Polarization structure of beam fanning in low-symmetry photorefractive crystals

Alexandr Volkov,[1,][*] Alexandr Shumelyuk,[1] Serguey Odoulov,[1] and Mirco Imlau[2]

[1]*Institute of Physics, National Academy of Sciences, Nauky Ave. 46, Kyiv 680028, Ukraine*
[2]*Fachbereich Physik, Universität Osnabrück, Osnabrück D-49076, Germany*
*Corresponding author: ajuvolkov@gmail.com

Beam fanning in low-symmetry photorefractive crystals features nonuniform angular distribution of linear polarization. We study this phenomenon experimentally in monoclinic $Sn_2P_2S_6$ crystals that belong to the m class of symmetry and compare the results with the predictions of a simple model that describes amplification of a weak scattered wave via nonlinear coupling to the intense incident wave.   © 2013 Optical Society of America

OCIS codes: 160.5320, 190.4223.

1. INTRODUCTION

Asymmetric wide-angle light-induced scattering or beam fanning is a typical feature of photorefractive crystals with sufficiently strong two-beam coupling. It originates from recording of spatially shifted index gratings and enhancement of the seeding light via self-diffraction from these gratings [1,2]. The spatial distribution of the scattered light is imposed by the angular dependence of the gain factor, which in turn depends on the effective electro-optic coefficient, including secondary contribution, caused by the piezoelectric and optoelastic effects [3,4].

Polarization of fanning light was never a subject of special investigation. It is generally believed that it does not depend on the scattering angle for optically isotropic crystals of cubic symmetry, sillenites (32 symmetry class), and semiconductors CdTe, GaAs ($\bar{4}3$ m symmetry class). For birefringent BaTiO₃ (4 mm symmetry class), LiNbO₃, or SrBaNbO₃ (3 m symmetry class), in commonly used y- or x-cut samples, the polarization of the beam fanning is nearly uniform, too. It corresponds to the polarization of the eigenwave that can be coupled the most efficiently to the incident light wave. Beam fanning can be caused by either of two eigenwaves, ordinary or extraordinary; however, in the second case, the scattering is stronger, owing to the particular hierarchy of the Pockels coefficients in these crystals.

It should be noted that even in 4 mm and 3 m photorefractive crystals, the polarization of fanning does not always coincide with that of the incident wave. A complicated distribution of polarization was observed in cross-like backscattering in z-cut LiNbO₃ [5,6], where the polarization vector of eigenwave depends on the scattering angle.

The nonuniform polarization of fanning, which is rather exceptional for 4 mm and 3 m photorefractive crystals, becomes a natural property for low-symmetry photorefractive crystals, for example, for monoclinic (m symmetry class) $Sn_2P_2S_6$ (SPS) crystals [7]. To a larger or smaller extent, the beam fanning polarization in these crystals is always spatially nonuniform, no matter the propagation direction of the light wave

coming from the outside (pump wave). This is a consequence of crystal biaxiality (with the two optical axes well separated spatially) and also of the fact that in monoclinic crystals the optical frame does not coincide with the crystallographic frame [8,9].

In this paper we describe experimental measurements of the polarization and intensity distributions of beam fanning in nominally undoped SPS and compare the results with those calculated within a simple two-beam coupling model that takes into account the particular anisotropic properties of the refractive indices, electro-optic coefficients, and charge screening effects.

After brief qualitative description of wide-angle photorefractive scattering and formulation of the main approximations valid for scattering in undoped SPS (Section 2), we describe the experimental procedure that allows for reconstructing the polarization structure of the scattered light on the screen behind the sample (Section 3), calculate the 2D maps of the angular distribution of scattering polarization (Section 4), and finally compare calculated and measured data (Section 5).

2. QUALITATIVE DESCRIPTION OF WIDE-ANGLE PHOTOREFRACTIVE SCATTERING

When a coherent light beam enters a photorefractive crystal, a part of its intensity is scattered from the bulk and surface optical imperfections of the sample. This scattered light is mutually coherent with the incident (pump), light and together they can write the index gratings, often called "noisy" gratings. In crystals with a nonlocal nonlinear response (charge transport driven by diffusion, charge hopping [10], or circular photovoltaic currents [11]), the weak scattered light can be amplified in the steady state because of self-diffraction from these noisy gratings. This results in wide-angle light-induced scattering called beam fanning, which is a subject of the present study with SPS.

Every spatial component of beam fanning originates only from the direct two-beam coupling of the seeding scattered

wave to the pump wave. No gain from parametric mixing of more than two waves is considered. This imposes the requirement that every particular scattered wave and pump wave are both the eigenwaves of the crystal. Otherwise, four-wave mixing of two pairs of eigenwaves [12] needs to be taken into account, which can result in enhanced scattering at special phase-matched directions. This topic is out of the scope of this paper.

Let the pump wave fall normally to the crystal cut. In undepleted pump approximation, the steady-state intensity I_s of the weak beam scattered inside sample at an angle θ_i to the normal of the input face grows exponentially

$$I_s(\ell) = I_{s0} \, \exp(\Gamma \ell) \qquad (1)$$

with the gain factor

$$\Gamma = \frac{2\pi}{\lambda \, \cos(\theta_i/2)} \, n_s n_p^2 r_{\mathrm{eff}} E_{\mathrm{sc}}, \qquad (2)$$

and space charge field

$$E_{\mathrm{sc}} = (\mathbf{e}_s \cdot \mathbf{e}_p) \frac{k_B T}{q} \frac{K_g}{1 + (K_g \ell_s)^2}. \qquad (3)$$

Here, the interaction length is ℓ, the Boltzmann constant is k_B, and the absolute temperature is T. The refraction indices are $n_{s,p}$, with subscripts s and p for the scattered and pump waves, respectively, λ is the recording light wave length, q is the electron charge, and the Debye screening length is

$$\ell_s = \sqrt{\frac{\epsilon \epsilon_0 k_B T}{q^2 N_{\mathrm{eff}}}} \qquad (4)$$

with dielectric permittivity $\epsilon \epsilon_0$ and effective trap density $N_{\mathrm{eff}} = (N_D - N_D^+) N_D^+ / N_D$; N_D and N_D^+ represent the total densities of donors and ionized donors, respectively. The grating spatial frequency

$$K_g = \frac{4\pi n_s}{\lambda} \, \sin \frac{\theta_i}{2} \qquad (5)$$

depends on the scattering angle θ_i inside the sample.

The effective Pockels coefficient

$$r_{\mathrm{eff}} = \mathbf{d}_p (\hat{r} \mathbf{k}_g) \mathbf{d}_s \qquad (6)$$

affects the efficiency of the scattered wave coupling to the pump wave, caused by the anisotropic phase grating of the space charge field. Here $\mathbf{k}_g$ is the grating unit vector, $\hat{r}$ is the standard Pockels tensor, and $\mathbf{d}_{s,p}$ are the electric displacement unit vectors.

One should expect the strongest scattering for those seeding components that profit from the highest amplification rate, i.e., possess the largest positive $\Gamma \ell$. As follows from Eqs. (2)–(4), the spatial distribution of Γ is mainly determined by the effective electro-optic constant r_{eff} and screening effects owing to the limited ℓ_s (see more in [13]).

For diffusion dominated charge transport, the largest gain factor Γ is achieved for identically polarized s and p waves, when the scalar product $(\mathbf{e}_s \cdot \mathbf{e}_p)$ takes its maximum value

equal to unity. That is why, quite often, the polarization of the beam fanning is practically uniform and identical to the polarization of the pump wave.

In low-symmetry crystals like SPS, in the general case, the scalar product $(\mathbf{e}_s \cdot \mathbf{e}_p)$ never equals unity because the polarization of the scattered eigenwave depends on the direction of its propagation and does not coincide with that of the pump wave. Thus, one can expect a considerable amplification for those noisy scattered components that are eigenwaves that belong to the same shell (inner or outer) of the normal surface in wavevector space and have the polarization that is closest to the linear polarization of the pump wave.

With the above assumption, the polarization structure of the beam fanning inside the sample should mimic the spatial distribution of the crystal eigenwave polarization. It should be underlined, however, that in the experiment scattered light is analyzed in the free space behind the sample. The polarization structure of this light is not the same as inside the sample, because it is affected by the polarization-sensitive reflection/refraction from the sample output face.

It will become clear from what follows that this contribution into polarization nonuniformity of scattered light is not negligible and modifies nonuniformity quite strongly, which is due to the low symmetry of the crystal itself.

3. EXPERIMENT

The experimental study of beam fanning is done with SPS crystals grown at Uzhgorod State University, Ukraine. The nominally undoped SPS sample is chosen with virtually no compensation grating (type II SPS; see [9]). An unexpanded light beam from the Kr$^+$ laser ($\lambda = 647$ nm, $I_p = 800$ mW) impinges upon the 12 mm thick y-cut sample nearly perpendicularly to its input face [see Fig. 1(a)]. The linear polarization of the incident beam is adjusted to be parallel to the short axes of the Fresnel index ellipsoid x_1 [14], i.e., making an angle $\psi_p = -47°$ with the x axis.

The polarizing sheet P is placed behind the sample. Its orientation is described by the angle ψ between its absorption axis and the x axis. So, when $\psi = \psi_p$, it stops the transmitted incident wave almost completely. After passing through the polarizing sheet P, the fanning light comes to the translucent
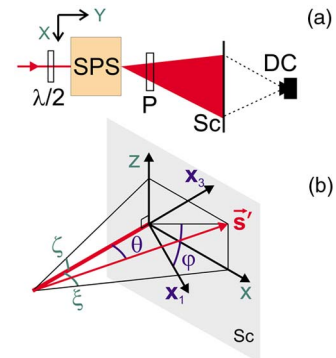

Fig. 1. (Color online) Schematic representation of the scattering geometry. (a) The light beam with polarization adjusted by half-wave plate $\lambda/2$ induces photorefractive scattering in SPS crystal. The intensity distribution of the beam fanning on the translucent screen Sc with the polarization selected by polarizer P is stored by camera DC. (b) The direction $\mathbf{s}'$ of any scattering ray in air is characterized by angles ξ and ζ in the crystallographic frame (x, y, z), while θ, φ are given in the optical frame (x_1, x_2, x_3) related to the optical indicatrix.

screen Sc, from where the intensity distribution is recorded with a digital camera (DC) that ensures a linear response to the light intensity within the working interval of exposures. To avoid overexposure from the transmitted beam (and to use more efficiently the dynamic range of the camera), this beam is directed into a small (7 mm in diameter) aperture in the screen.

The distance from the sample (SPS) to the screen (Sc) is 10 cm. Thus, the light pattern on the screen represents the angular distribution of scattered intensity (far field). Any spot on the screen is characterized by the Cartesian coordinates ξ and ζ, which are measures of horizontal angular deviation of the scattered component from the yz plane and vertical angular deviation from the xz plane, respectively. The screen collects all light components scattered in air within the angular window $\xi \in [-10°, 60°]$ and $\zeta \in [-30°, 30°]$ in horizontal and vertical directions, respectively.

The steady-state intensity distribution recorded from the screen is shown in Fig. 2(a) for the case of no polarization filtering and in Fig. 2(b) for the polarizing sheet placed between the sample and the screen and adjusted to cut off the light with the polarization azimuth $\psi = -42°$. The scattering pattern has a typical petal shape, which is aligned, in the case of nominally undoped SPS, in the positive direction of the sample x axis.

The curved dark stripe is clearly seen in the pattern with partially filtered polarization [Fig. 2(b)], while it is absent in pattern of Fig. 2(a) taken with no polarization filtering. This difference confirms the nonuniform polarization structure of the beam fanning. The position of the dark stripe depends on the polarizer adjustment angle: with increasing ψ, the stripe moves out of the position of transmitted laser beam on the screen.

The polarization structure of the beam fanning pattern is reconstructed via digital processing of the images like that shown in Fig. 2(b), recorded with a DC for several different
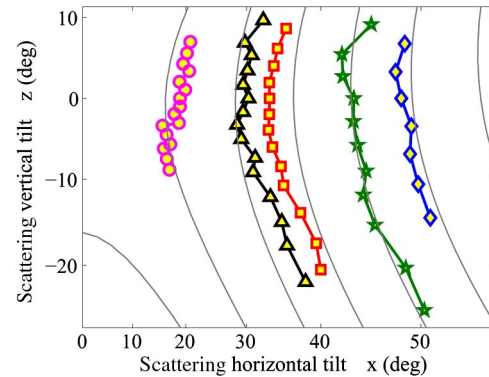
Fig. 3.   (Color online) Polarization distributions of the fanning light on the screen induced by a laser beam with polarization angle $\psi_p = -47°$. Circles, triangles, squares, pentagrams, and diamonds denote measured spatial distributions of scattered light polarization angles $\psi = -46°$, $-44°$, $-42°$, $-40°$, and $-38°$. The thin gray lines show calculated data for the same set of polarization angles.

orientations of the polarizer. For each pattern, we seek to trace the line along which the scattered wave polarization is parallel to the polarizer absorption axis.

The details of the polarization data processing are given in the Appendix A. The whole procedure is based on several assumptions, some related to the experimental conditions, the others to the inherent optical and photorefractive properties of SPS. The most serious but justified approximations are as follows: (i) the transmission and absorption of the polarizer sheet do not change for off-normal beams in the studied range of angles, (ii) owing to a relatively high index of refraction ($n \approx 3$), all scattering angles inside the sample are small, $\theta_i \leq 17°$, (iii) within the angular window where measurements are done, $15° \leq \theta \leq 60°$, the intensity of scattered light decreases nearly exponentially with the scattering angle in air, $I_s \propto \exp(-b\theta)$.

Figure 3 shows the polarization structure of the beam fanning for the incident beam, which is polarized along the small axis of the optical indicatrix ($\psi_p = -47°$). The dots connected by the solid lines correspond to the discrete rotations of the polarizing sheet, every time to 2° (except the first step with angular separation of 1°). The variation of the polarization angle from $-47°$ to $-35°$ was detected easily. The thin solid lines in Fig. 3 represent the results of polarization structure calculation, as will be discussed in the next section.

Within our experimental accuracy, any nonuniformity in the scattered light polarization has been detected when the incident laser beam is polarized along the big axis of the optical indicatrix ($\psi_p = 43°$). For a pump wave entering the x face or the z face of the sample, the polarization of scattering light was also nearly spatially uniform.

4. CALCULATION OF POLARIZATION DISTRIBUTION IN THE SCATTERING PATTERN

To give a description of the polarization inhomogeneity of the scattering pattern and to reveal the origin of the quantitative difference in patterns for two orthogonally polarized pump waves, a simple model is considered, with two important consecutive steps. First, the polarization of scattered light inside the sample is found under the assumption that it should coincide with the polarization of the crystal eigenwave whose
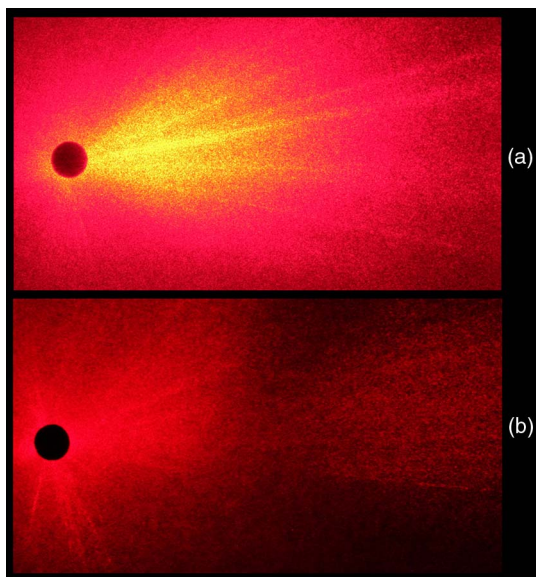

Fig. 2.   (Color online) Scattered light patterns on the screen recorded with the DC: (a) with no polarizer between the sample and the screen, and (b) with polarizer adjusted to cut the light with the polarization azimuth $\psi = -42°$. The horizontal width of each frame makes 70°.

polarization is close to that of the pump. Second, the change of polarization due to reflection/refraction from the output face of the sample is accounted for to get the polarization distribution on the observation screen.

Thus, in spite of the fact that beam fanning is a typical example of nonlinear scattering, the calculation of its polarization structure is reduced to the problem of linear optics. (The nonlinearity starts, however, to be very important when it becomes necessary to estimate the spatial dependences of the scattered intensity, as explained in the Appendix A.)

The polarization of the crystal eigenwave with the unit wavevector $\mathbf{s} = \mathbf{k}/k$ can be found from the wave equation

$$[\mathbf{s}, [\mathbf{s}, \hat{B}\mathbf{d}]] + \mathbf{d}n^{-2} = 0, \tag{7}$$

where $\mathbf{d}$ is the unit displacement vector, later called the polarization vector, and $\hat{B}$ is the dielectric impermeability tensor. This tensor is reduced to diagonal form in the optical frame, i.e., the Cartesian coordinates (x_1, x_2, x_3) that coincide with the axes of the optical indicatrix. As mentioned already, the optical frame does not coincide with the crystallographic frame [9]. Only the x_2 axis is parallel to the crystallographic y axis, while the x_1 axis makes the angle $-47°$ with the crystallographic x axis [Fig. 1(b)].

Even within the optical frame, the expression for the spatial distribution of $\mathbf{d}$ is quite cumbersome. It can be simplified, however, provided the scattering angles θ_i inside the sample are small. The wave that propagates in the direction

$$\mathbf{s} = \begin{pmatrix} \theta_i \cos \varphi \\ 1 - \frac{1}{2}\theta_i^2 \\ \theta_i \sin \varphi \end{pmatrix} \tag{8}$$

may have, as follows from Eq. (7), one of the two eigenpolarizations

$$\mathbf{d}_1 = \begin{pmatrix} 1 - \frac{1}{2}\theta_i^2 \cos^2 \varphi \\ -\theta_i \cos \varphi \\ (\kappa - \frac{1}{2})\theta_i^2 \sin 2\varphi \end{pmatrix}, \qquad \mathbf{d}_3 = \begin{pmatrix} -\kappa\theta_i^2 \sin 2\varphi \\ -\theta_i \sin \varphi \\ 1 - \frac{1}{2}\theta_i^2 \sin^2 \varphi \end{pmatrix}, \tag{9}$$

where $\mathbf{d}_1$ and $\mathbf{d}_3$ are closest to the axes $\mathbf{x}_1$ and $\mathbf{x}_3$, respectively, and the azimuth angle φ is counted from the x_1 axis. The information on the crystal's optical indicatrix enters Eq. (9) via the factor

$$\kappa = \frac{n_1^2(n_3^2 - n_2^2)}{2n_2^2(n_3^2 - n_1^2)} = \frac{1}{1 - \cos 2V}, \tag{10}$$

which is related to the angle $2V$ between the optical axes of the crystal. They take, with $n_1 = 3.00$, $n_2 = 2.91$, and $n_3 = 3.07$ at $\lambda = 647$ nm [14], the values $2V = 79°$ and $\kappa = 1.2$.

With the known spatial distribution of the polarization inside the sample, given by Eq. (9), it is possible to evaluate now its modification, which is due to the refraction and reflection from the crystal output face.

In general, when an arbitrary polarized wave comes from the birefringent medium to the interface with the optically isotropic medium, it is transformed into two reflected waves and one transmitted wave. Our estimates show that the angular splitting of the two reflected waves makes less than 12% of scattering angle θ_i inside the sample and does not exceed

1.6° for the largest one. This is a reason for neglecting the spatial separation of the reflected waves and, thus, reducing the problem to refraction/reflection from the interface of two isotropic media (in spite of the obvious anisotropy of our low-symmetry sample).

From the Fresnel equation for the isotropic medium, it follows that the polarization azimuth (i.e., the angle between the polarization vector $\mathbf{d}$ and the plane of incidence) of the wave changes from α to α' when passing the interface

$$\tan \alpha' = \cos(\theta - \theta_i) \tan \alpha, \tag{11}$$

where θ is the scattering angle in air. Inside the sample the polarization azimuth α depends on the polarization direction and plane of incidence orientation (which is imposed by the direction of scattered beam $\mathbf{s}$). With the known in-plane $d_\parallel$ and out-of-plane $d_\perp$ projections of the polarization vector $\mathbf{d}$, the polarization azimuth $\alpha = \arg(d_\parallel + id_\perp)$ is found. According to Eq. (11), the polarization azimuth outside the sample is not bigger than inside. By using the Snell law, the direction $\mathbf{s}'$ of the scattered wave in air is found and described by the angles ξ and ζ. Then the polarization direction $\mathbf{d}'$ in air is reconstructed with the known plane of incidence and polarization azimuth α'.

Finally, the group of scattered waves that should be cut off by a polarizer is found. The angle ψ of the polarizer determines the absorption axis direction

$$\mathbf{p} = \mathbf{x} \cos \psi + \mathbf{z} \sin \psi. \tag{12}$$

The dependence of the polarizer absorption on the angle of incidence of the scattered component is assumed to be weak. This approximation is equivalent to the requirement that all scattered components propagate inside the polarizer roughly along to the normal of its surface. Neglecting the reflection from its surface, the ray polarization direction inside the polarizer transforms to

$$\mathbf{d}'' = \{(\mathbf{y} \cdot [\mathbf{s}', \mathbf{d}'])[\mathbf{s}', \mathbf{y}] + (\mathbf{y} \cdot \mathbf{d}')[[\mathbf{s}', \mathbf{y}], \mathbf{y}]\}[\mathbf{s}', \mathbf{y}]^{-2}. \tag{13}$$

The polarizer adjusted at the angle ψ stops a group of scattered waves that meet the condition $\mathbf{d}'' = \mathbf{p}$.

The 2D map that represents the spatial distribution of the polarization angle ψ is shown in Fig. 4 for the incident wave polarized along the small axis of the indicatrix. The
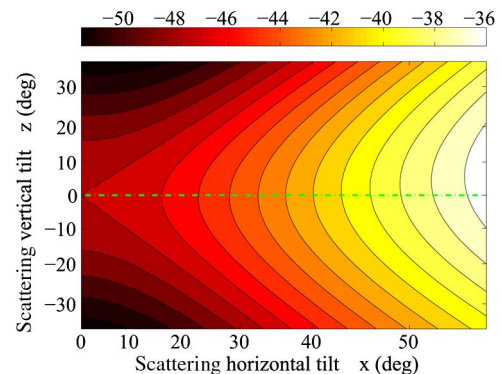

Fig. 4. (Color online) Calculated distribution of the polarization angle ψ of scattering rays produced by the incident wave with polarization angle $\psi_p = -47°$.
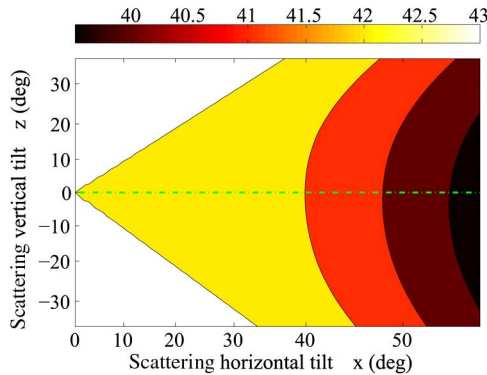
Fig. 5.   (Color online) Calculated distribution of the polarization angle ψ of scattering rays produced by the incident wave with polarization angle $\psi_p = 43°$.

polarization angle ψ is coded here by the gray color density (by different colors in online publication), with the scale given in the horizontal bar above the main frame. The black lines with identical polarization are plotted for the discrete values of ψ, separated by 1° from each other.

One particularity of this pattern that attracts attention is the presence of two straight black lines crossing at (0, 0) point. They are tilted to –47° and 43° with respect to the sample x axis; i.e., the light rays propagate there in the principal planes of the optical indicatrix. Thus, the polarization of these rays by definition can be either parallel or perpendicular to the plane itself. The refraction on the crystal surface and on the polarizer surface does not change the polarization of these rays. The other fact that can be easily seen from Fig. 4 is a slight asymmetry of the calculated polarization distribution against the horizontal line ($\zeta = 0$).

Figure 5 shows the polarization distribution map for the pump wave with orthogonal polarization (along the long axis of the indicatrix). It contains two similar orthogonal lines crossing at the (0, 0) point, and it is also asymmetric with respect to the horizontal line. The spatial variations of the polarization, however, are much more modest as compared to those shown in Fig. 4.

5. DISCUSSION

The changes in the position and the shape of the dark stripe on the screen when the polarizer is rotated are similar to the changes in the principal isogyres in the conoscopic pattern when rotating crossed polarizers [15, Chapter 14.4]. The light scattered inside the sample produces the diverging beam and the polarization-dependent light amplification in photo-refractive crystal acts as an input polarizer, thus leading to similarity between these two phenomena. The essential difference of the described polarization pattern from the conoscopic pattern consists in the absence of isochromates, since wide-angle photoinduced scattering is formed by waves that belong to only one optical mode (one and the same crystal eigenmode).

Comparison of the data presented in Figs. 4 and 5 shows a quite different variation of the polarization of the fanning light within the same angular window. Much more rapid variation of the polarization is observed for the incident wave polarized along the x_1 axis of the index ellipsoid. As already mentioned, the nonuniform spatial distribution of the polarization on the

screen has two origins, one related to the optical anisotropy of the crystal and the other due to modification of polarization on the crystal–air interface. It appears that modification of the polarization at the interface enhances the already existing nonuniformity of the polarization for the pump wave with smaller index n_1 and inhibits these variations for the pump wave with the larger index n_3.

This difference can be explained qualitatively by the addition or subtraction of two—above-mentioned—effects that lead to polarization nonuniformity. When the scattering angle θ of the eigenwave with small refractive index increases, the polarization direction deviates from the x_1 axis to the y axis coming to the plane of incidence. Such a decrease in the polarization azimuth is sped up by refraction at the sample output face, according to Eq. (11). On the contrary, in the case of the orthogonally polarized eigenwave, the refraction inhibits the growth of the polarization azimuth with the angle θ.

It should be underlined that the polarization nonuniformity becomes especially strong if the optical indicatrix is tilted considerably with respect to the principal direction of nonlinear scattering (beam fanning). It follows from Eq. (11) that for small θ_i,

$$\Delta\alpha = \alpha - \alpha' \approx \sin^2 \frac{\theta - \theta_i}{2} \sin 2\alpha. \tag{14}$$

The changes in the polarization azimuth $\Delta\alpha$ become larger when increasing the scattering angle θ and the index of refraction. The largest changes in the polarization azimuth occur in the vicinity of $\alpha = 45°$. This is just the case of SPS crystal in which the petal of the beam fanning is aligned nearly along the crystallographic x axis (see Fig. 2), while the eigenwave polarizations in the y-cut sample make the angles roughly $\pm 45°$ to the x axis.

Qualitatively different is the scattering in the z-cut sample where the polarization of the eigenwave either coincides or makes 90° with respect to the fanning direction. The expected polarization changes in the scattering pattern are so small that they were not detected experimentally.

When the scattering angle increases, the higher terms in the series expansion of Eq. (14) need to be taken into account. In this case the largest change in the azimuth $\Delta\alpha$ occurs at higher values of the azimuth (up to $\alpha \approx 60°$). Visually it manifests itself in a slight deviation of the polarization angle gradient in Figs. 4 and 5 from the horizontal line.

To compare the experimental data for SPS with our expectations, gray curves are plotted in Fig. 3 that represent the location of the scattered components with identical polarization. Calculation was performed with discrete polarizer tilt angles ψ_p that match the values choosen in the experiment. The qualitative agreement is evident: the shape, the curvature, and the orientation of the measured curves with identical polarization agree satisfactory with those calculated. The semi-quantitative agreement can also be stated: the positions of measured and calculated lines in the 2D map of Fig. 3 also agree satisfactorily.

A much smaller spatial variation of scattered light polarization calculated for the pump wave polarized along the x_3 direction of the optical indicatrix explains the fact that the experimental accuracy of the polarization mapping did not allow for detecting these variations.

6. CONCLUSIONS

The nonuniform spatial distribution of polarization within the wide-angle light-induced scattering (beam fanning) in monoclinic photorefractive crystal SPS is studied experimentally and shown to agree satisfactorily with the results of the performed calculations.

It is shown, in particular, that two processes feed this non-uniformity, both resulting in variations of polarization, comparable in value. The first consists in a change of eigenwave polarizations with their direction of propagation in the crystal. The second is a consequence of polarization filtering when the scattered component passes a sample/air interface.

The two mentioned sources of polarization nonuniformity are especially pronounced in SPS because its refractive index is big and the optical indicatrix is aligned roughly along the bisectrix of the crystallographic axes x and z.

It seems the second origin of polarization nonuniformity is universal and should manifest itself also in classical photorefractive crystals such as $BaTiO_3$ (4 mm symmetry class) and $LiNbO_3$ (3 m symmetry class). It is, however, practically unimportant for the mentioned two crystals where the optical frame coincides with the crystallographic frame and the dielectric frame. The largest gain factor (and thus the largest scattered intensity) occurs along the crystallographic z axis, which is also the axis of the optical indicatrix. Possible variations in polarization could be expected in these crystals for quite different directions, somewhere between the crystallographic axes z and x (or z and y), i.e., in the directions where the fanning is very small.

APPENDIX A: POLARIZATION DATA PROCESSING

Comparing the scattering patterns of the two frames of Fig. 2, one can detect the presence of the dark stripe in Fig. 2(b). Each of its points is a local minimum of brightness of the screen in the transverse direction. This minimum of brightness never goes down to exact zero because of residual transmission of the polarizer. Therefore the considerable (up to one order in magnitude) decrease in the scattering intensity with angle θ distorts the cross-sectional profile of the dark stripe and shifts it toward larger angles θ. We exclude such distortion by dividing the distribution of brightness by the distribution of scattering intensity.

The dependence of the scattering intensity on the polar angle θ can be approximated by an exponential function in
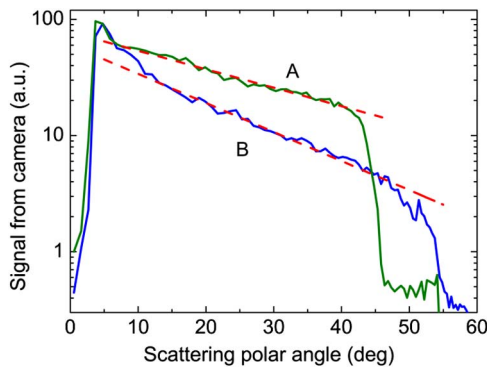
Fig. 6.   (Color online) Scattered intensity versus scattering angle measured along two straight lines with constant polarization $\varphi = 0$ (curve A) and $\varphi = 90°$ (curve B) shown in Fig. 4.
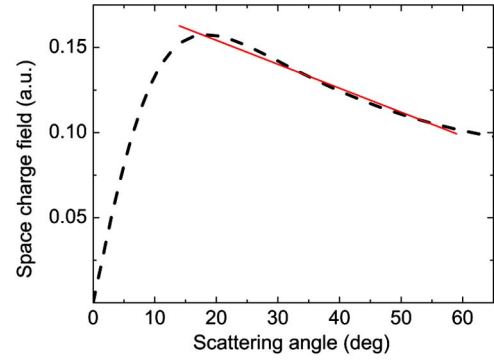
Fig. 7.   (Color online) Angular dependence of the space charge field calculated for $\lambda = 647$ nm and $2\pi\ell_s = 2$ µm (doted line) and its linear approximation in an angular range from $15°$ to $60°$ (red solid line).

wide angular range, as can be clearly seen for two azimuth sections of the intensity distribution (Fig. 6).

At first glance, this looks strange because this dependence is given by quite complicated expressions for the gain factor, Eqs. (1)–(6). For relatively small spatial frequencies, these equations predict, in particular, linear increase of the gain factor with θ, imposed by the increasing diffusion field. However, with the pronounced charge screening in SPS [13] taken into account, we conclude that the main contribution to the angular dependence of E_s, Γ, and finally I_s comes from the denominator of Eq. (3). The approximate function

$$\ln I_s(\theta) \propto \Gamma(\theta) \propto E_s(\theta) \propto \frac{\sin \theta}{1 + (2\pi\ell_s/\lambda)^2 \sin^2 \theta} \quad \text{(A1)}$$

differs from

$$\ln I_s(\theta) = a - b\theta \quad \text{(A2)}$$

only for 5% within the θ range from $15°$ to $60°$, where all our measurements were done, as illustrated in Fig. 7.

The constant parameter a does not influence the dark stripe position and can be omitted. The parameter b in Eq. (A2) depends on the azimuth angle φ. In our calculations we use an average value of parameter $b = 2.7$ rad^{-1} because mismatch of this parameter does not exceed 20%. So, multiplying the brightness of each screen point on factor $\exp(2.7\theta)$, where θ is a polar angle of the point, we obtain a function that describes the angular distribution of the polarization only. Its minimum shows a set of beams with polarization angle ψ that is equal to the angle ψ_p of the polarizer. By analyzing the set of pictures stored with different values of ψ_p, the distribution of polarization angle shown in Fig. 3 was obtained.

REFERENCES

1. V. V. Voronov, I. R. Dorosh, Y. S. Kuz'minov, and N. V. Tkachenko, "Photoinduced light scattering in cerium-doped

barium strontium niobate crystals," Sov. J. Quantum Electron. **10**, 1346–1349 (1980).

2. J. Feinberg, "Asymmetric self-defocusing of an optical beam from the photorefractive effect," J. Opt. Soc. Am. **72**, 46–51 (1982).

3. S. Stepanov and M. Petrov, "Nonstationary holographic recording for efficient amplification and phase conjugation," in *Photorefractive Materials and Their Applications I: Fundamental Phenomena*, P. Günter and J.-P. Huignard, eds. Vol. **61** of Topics in Applied Physics (Springer-Verlag, 1988), pp. 263–289.

4. G. Montemezzani, A. A. Zozulya, L. Czaia, D. Z. Anderson, M. Zgonik, and P. Günter, "Origin of the lobe structure in photorefractive beam fanning," Phys. Rev. A **52**, 1791–1794 (1995).

5. R. Grousson, S. Mallick, and S. Odoulov, "Amplified backward scattering in LiNbO$_3$:Fe," Opt. Commun. **51**, 342–346 (1984).

6. V. Obukhovsky, S. Odoulov, and S. Karabekian, "Backward conical photorefractive scattering in LiNbO$_3$," Opt. Commun. **104**, 123–128 (1993).

7. A. Shumelyuk, A. Volkov, A. Selinger, M. Imlau, and S. Odoulov, "Frequency-degenerate nonlinear light scattering in low-symmetry crystals," Opt. Lett. **33**, 150–152 (2008).

8. B. Boulanger, Y. Petit, P. Segonds, C. Félix, B. Ménaert, J. Zaccaro, and G. Aka, "Absorption and fluorescence anisotropies of monoclinic crystals: the case of Nd:YCOB," Opt. Express **16**, 7997–8002 (2008).

9. A. Grabar, M. Jazbinšek, A. Shumelyuk, Y. Vysochanskii, G. Montemezzani, and P. Günter, "Photorefractive effects in Sn$_2$P$_2$S$_6$," in *Photorefractive Materials and Their Applications 2: Materials*, P. Günter and J.-P. Huignard, eds. Vol. **114** of Springer Series in Optical Sciences (Springer, 2007), pp. 327–362.

10. L. Solymar, D. J. Webb, and A. Grunnet-Jepsen, *The Physics and Applications of Photorefractive Materials*, Vol. **11** of Oxford Series in Optical and Imaging Sciences (Oxford University, 1996).

11. A. Novikov, S. Odoulov, O. Oleinik, and B. Sturman, "Beam-coupling, four-wave mixing and optical oscillation due to spatially-oscillating photovoltaic currents in lithium niobate crystals," Ferroelectrics **75**, 295–315 (1987).

12. B. Sturman, S. Odoulov, and M. Goulkov, "Parametric four-wave processes in photorefractive crystals," Phys. Rep. **275**, 197–254 (1996).

13. A. Shumelyuk, A. Volkov, S. Odoulov, G. Cook, and D. Evans, "Coupling of counterpropagating light waves in low-symmetry photorefractive crystals," Appl. Phys. B **100**, 101–108 (2010).

14. D. Haertle, A. Guarino, J. Hajfler, G. Montemezzani, and P. Günter, "Refractive indices of Sn$_2$P$_2$S$_6$ at visible and infrared wavelengths," Opt. Express **13**, 2047–2057 (2005).

15. M. Born and E. Wolf, *Principles of Optics: Electromagnetic Theory of Propagation, Interference and Diffraction of Light* (Cambridge University, 1999).